



Kent Academic Repository

Wu, Liang, Shen, Yiting, Zhang, Zaichen, Dang, Jian, Liu, Huaping and Wang, Jiangzhou (2020) *Receiver Algorithms for Single-Carrier OSM Based High-Rate Indoor Visible Light Communications*. *IEEE Transactions on Wireless Communications* 19 (2). pp. 1113-1126. ISSN 1536-1276.

Downloaded from

<https://kar.kent.ac.uk/81072/> The University of Kent's Academic Repository KAR

The version of record is available from

<https://doi.org/10.1109/TWC.2019.2951148>

This document version

Author's Accepted Manuscript

DOI for this version

Licence for this version

UNSPECIFIED

Additional information

Versions of research works

Versions of Record

If this version is the version of record, it is the same as the published version available on the publisher's web site. Cite as the published version.

Author Accepted Manuscripts

If this document is identified as the Author Accepted Manuscript it is the version after peer review but before type setting, copy editing or publisher branding. Cite as Surname, Initial. (Year) 'Title of article'. To be published in *Title of Journal*, Volume and issue numbers [peer-reviewed accepted version]. Available at: DOI or URL (Accessed: date).

Enquiries

If you have questions about this document contact ResearchSupport@kent.ac.uk. Please include the URL of the record in KAR. If you believe that your, or a third party's rights have been compromised through this document please see our [Take Down policy](https://www.kent.ac.uk/guides/kar-the-kent-academic-repository#policies) (available from <https://www.kent.ac.uk/guides/kar-the-kent-academic-repository#policies>).

Receiving Algorithms for Single-Carrier OSM Based High-Rate Indoor Visible Light Communications

Liang Wu, *Member, IEEE*, Yiting Shen, Zaichen Zhang, *Senior Member, IEEE*,
Jian Dang, *Member, IEEE*, Huaping Liu, *Senior Member, IEEE*, and Jiangzhou
Wang, *Fellow, IEEE*

Abstract

In intensity-modulation and direct-detection (IM/DD) multiple-input and multiple-output (MIMO) visible light communication (VLC) systems, spatial subchannels are usually correlated, and spatial modulation is a good choice to achieve the advantages of MIMO technology. Peak-to-average power ratio (PAPR) is a key issue in VLCs due to the limited linear dynamic range of light emitting diodes (LEDs). Single-carrier communication systems have a lower PAPR than orthogonal frequency division multiplexing (OFDM) communication systems. However, it is challenging to design a single-carrier spatial modulation for high-rate transmissions because of the time domain intersymbol interference. This paper develops an optical spatial modulation (OSM) scheme based on bipolar pulse amplitude modulation (PAM) and spatial elements for high-rate indoor VLC systems. Multiple data streams can be transmitted simultaneously in the proposed scheme. Based on the transmit strategy, we develop a low-complexity receive algorithm that achieves better bit-error rate performance than reference schemes, and the proposed OSM scheme has a much lower PAPR than OFDM based OSM schemes. When the spatial subchannels are highly correlated, a spatial area division strategy is applied, and the receive

L. Wu, Y. Shen, Z. Zhang and J. Dang are with National Mobile Communications Research Laboratory, Southeast University, Nanjing 210096, China (e-mail: {wuliang, ytshen, zczhang, dangjian}@seu.edu.cn).

H. Liu is with the School of Electrical Engineering and Computer Science, Oregon State University, Corvallis, Oregon 97331, USA (e-mail: hliu@eeecs.oregonstate.edu).

J. Wang is with School of Engineering and Digital Arts, University of Kent, Canterbury, CT2 7NT United Kingdom (e-mail: j.z.wang@kent.ac.uk)

algorithm is investigated. The symbol-error rate expression of the proposed OSM scheme is derived, and the computational complexity is analyzed.

Index Terms

High rate, optical spatial modulation (OSM), pulse-amplitude modulation (PAM), visible light communication (VLC).

I. INTRODUCTION

Visible light communication (VLC) has received increasing attention in both academia and industry due to the low cost and long lifetime of light emitting diodes (LEDs) [1], [2]. Large unregulated spectrum, high data rate, and high data security are the main advantages of VLCs. The most commonly used scheme for VLC systems is intensity modulation paired with direct detection (IM/DD) [3], [4]. With IM/DD, the transmitted signals must be nonnegative. Consequently, most RF modulation schemes cannot be directly used for IM/DD VLCs. DC-biased and non-DC-biased modulation schemes have been proposed for IM/DD VLCs [5], [6].

Although there is a large amount of unregulated visible light spectrum, the 3-dB modulation bandwidth of LED is only tens of MHz. Therefore, there exists intersymbol interference (ISI) in high-rate transmissions. To achieve a high data rate and combat ISI, researchers have investigated multicarrier modulation schemes for VLCs. DC-biased optical orthogonal frequency division multiplexing (DCO-OFDM) is a multicarrier modulation scheme, where the frequency domain signals are hermitian symmetric and a DC bias is added to the time domain signal to satisfy the IM/DD constraint [7]. Asymmetrically clipped optical OFDM (ACO-OFDM) is a unipolar form of OFDM, where no DC bias is needed and only odd subcarriers are used [8]. The performance of ACO-OFDM was evaluated in [9], and the power efficiency of ACO-OFDM is higher than that of DCO-OFDM [10]. Pulse amplitude modulation modulated discrete multitone (PAM-DMT) modulates only the imaginary parts of the subcarriers, and the the entire negative excursion is clipped [11]. The performances of the three OFDM schemes were analyzed in [12]. PAM-DMT and flip-OFDM [13] achieve the same optical power and spectral efficiencies as ACO-OFDM. Beside, the single carrier modulation based frequency domain equalization (FDE) schemes can also be employed to combat ISI. A DC-biased PAM based frequency domain equalization (FDE) scheme for VLCs was evaluated in [5].

To further improve the data rate of VLCs, multiple-input multiple-output (MIMO) technology is employed. MIMO technology can efficiently improve the spectral efficiency and mitigate the bandwidth limitation set mainly by the LED. The schemes in [14], [15] investigated the multiplexing gain of MIMO optical wireless communication systems. Modified Alamouti code employing ACO-OFDM was proposed in [16], which showed that the performance of Alamouti code in optical wireless systems is independent of the delay difference between the two paths. The use of Alamouti code with DCO-OFDM was investigated in [17]. The schemes in [16] and [17] investigated the methods to exploit diversity gain of MIMO systems. Spatial modulation is another form to exploit the gain of multiple spatial elements [18]. The spatial subchannels in MIMO VLC systems employing a non-imaging receiver are usually correlated [15], and spatial modulation is more robust to high channel correlation [19]. An optical spatial modulation scheme (OSM) was proposed in [20], [21]. The transmit scheme of OSM is simple, but the optimal detection is complicated. A quad LED scheme and a dual-LED scheme were proposed for the IM/DD VLCs [22], [23]. These two schemes are the forms of OSM. The maximum likelihood (ML) detection algorithm with a high computational complexity was applied in [22] and [23] to achieve good performance. A low complexity optical spatial modulation was proposed in [24]. High-rate transmission is a key advantage of VLCs. In the high-rate transmission, ISI exists. However, the effect of ISI was not taken into account in these works [22]–[24].

OFDM based spatial modulation schemes are used to combat ISI, and the optimal detector can be applied in the frequency domain [25], [26]. Our previous work [27] has investigated a low complexity OFDM VLC system, where an OFDM based spatial modulation was proposed for diffuse environments. The system achieves the same error performance as ACO-OFDM or PAM-DMT schemes, but with a lower computational complexity. The principle in [27] was also studied independently in [28], where a non-DC-biased OFDM optical wireless system with a zero-forcing (ZF) receiver was used. Compared with multicarrier systems, single carrier systems have a lower peak-to-average power ratio (PAPR). PAPR is an important indicator in VLCs, as the linear dynamic range of LED is limited. However, it is challenging to efficiently combine the single carrier modulation with the time-domain spatial modulation in high-rate transmissions, because ISI exists in the time domain [29].

In this paper, by employing spatial elements, we propose a single-carrier OSM scheme named bipolar PAM based OSM for the high-rate IM/DD VLC, and spatial shift keying is applied based

on the polarity information of the PAM symbols. An equivalent channel is formed according to the properties of the transmitted signal, and a novel receive algorithm with a low computational complexity is proposed to combat ISI. When the spatial subchannels are highly correlated, a spatial area division strategy is applied to reduce the effect of the high correlation, and the receive algorithm is investigated. Compared with reference schemes, the proposed bipolar PAM based OSM scheme achieves better bit error rate (BER) performance. Besides, the PAPR of the proposed bipolar PAM based OSM scheme is much lower than that of the OFDM based OSM scheme. The advantages of the proposed scheme are validated via analytical symbol error rate (SER) as well as the simulated SER and BER results.

The main contributions of this paper include:

- 1) By employing bipolar PAM based OSM scheme, we consider a high-rate VLCs, where multiple data streams can be transmitted at the same time and the effect of ISI is considered. The constellation diagram of PAM is redesigned to improve the BER performance.
- 2) Based on the transmit strategy, a novel low complexity receive algorithm is proposed for the high-rate transmission. The SER and the computational complexity of the proposed bipolar PAM based OSM scheme are analyzed in detail.
- 3) When the correlation of spatial subchannels is high, a spatial area division strategy is applied and the receive algorithm is investigated. We compare the BER performance of the schemes with and without the spatial area division strategy.
- 4) Simulation results are provided, which show that the proposed bipolar PAM based OSM scheme can achieve better BER performance than reference schemes. Besides, the proposed scheme has a low PAPR.

The rest of the paper is organized as follows. In Section II, the channel model is presented. Section III presents the transmit strategy of the proposed bipolar PAM based OSM scheme. In Section IV, a low-complexity receive algorithm is proposed, and SER and computational complexity are analyzed. In Section V, the spatial area division strategy is applied for the highly correlated environment, and the receive algorithm is investigated. Simulation results are provided in Section VI to validate the proposed schemes, and the paper is concluded in Section VII.

II. CHANNEL MODEL

In the proposed bipolar PAM based OSM scheme, a point-to-point indoor MIMO VLC channel with n_t (n_t is an even integer) transmit LEDs and n_r receive PDs is considered. The LEDs are divided into several groups, and each LED group can have more than two LEDs. To achieve a high data rate, the transmit LEDs are divided into $n_t/2$ groups, and each group has two LEDs. The $n_t/2$ independent data streams can be transmitted at the same time. The indoor VLC channel consists of a LOS component and a diffuse component. The physical channel impulse response from the l -th LED of the j -th group to the k -th PD can be expressed as [30]

$$q_{k,(j,l)}(t) = \mu_k \eta_{\text{LOS}(k,(j,l))} \delta(t) + \mu_k q_{\text{diffuse}(k,(j,l))}(t - \Delta\tau_{k,(j,l)}), \quad (1)$$

where μ_k is the responsivity of the k -th PD, $\delta(t)$ is the dirac delta function, $q_{\text{diffuse}(k,(j,l))}(t)$ is the diffuse component of the physical channel from the l -th LED of the j -th group to the k -th PD, $\Delta\tau_{k,(j,l)}$ is the delay between the LOS signal and the onset of the diffuse signal, and $\eta_{\text{LOS}(k,(j,l))}$ is the LOS component from the l -th LED of the j -th group to the k -th PD and can be calculated according to the properties and the positions of LED and PD as [1]

$$\eta_{\text{LOS}(k,(j,l))} = \begin{cases} \frac{(m_{(j,l)}+1)A_{r,k} \cos(\varphi_{k,(j,l)})}{2\pi D_{k,(j,l)}^2} \cos^{m_{(j,l)}}(\phi_{k,(j,l)}) & 0 \leq \varphi_{k,(j,l)} \leq \Psi_k \\ 0 & \varphi_{k,(j,l)} > \Psi_k, \end{cases} \quad (2)$$

where $m_{(j,l)}$ is the order of Lambertian emission, which is related to $\Phi_{1/2,(j,l)}$ as

$$m_{(j,l)} = -\ln 2 / \ln(\cos \Phi_{1/2,(j,l)}), \quad (3)$$

where $\Phi_{1/2,(j,l)}$ is the semiangle at half-power of the l -th transmit LED in the j -th group, $\phi_{k,(j,l)}$ is the angle of irradiance from the l -th LED of the j -th group to the k -th PD, $A_{r,k}$ is the receive area of the k -th PD, $D_{k,(j,l)}$ and $\varphi_{k,(j,l)}$ are, respectively, the distance and angle of incidence from the l -th LED of the j -th group to the k -th PD, Ψ_k is the field of view (FOV) of the k -th PD.

In the frequency domain, the diffuse component is [30]

$$Q_{\text{diffuse}(k,(j,l))}(f) = \frac{\eta_{\text{diffuse}(k,(j,l))}}{1 + j \frac{f}{f_{0,(k,(j,l))}}}, \quad (4)$$

where $f_{0,(k,(j,l))}$ is the 3-dB cut off frequency, and $\eta_{\text{diffuse}(k,(j,l))}$ is expressed as

$$\eta_{\text{diffuse}(k,(j,l))} = \frac{A_{r,k}}{A_{\text{room}}} \frac{\rho_{1,(k,(j,l))}}{1 - \rho}, \quad (5)$$

where A_{room} is the area of the room surface, $\rho_{1,(k,(j,l))}$ is the reflectivity of the region initially illuminated by the l -th LED of the j -th group, and ρ is the average reflectivity of the walls. As adopted in [30], $\rho_{1,(k,(j,l))} = \rho$ is assumed in this paper.

The channel frequency selectivity of indoor VLCs was investigated in [31], which showed that the channel frequency selectivity arises mainly from the multiple LOS paths rather than diffuse propagation. In the high-rate transmission, the ISI is caused mainly due to the limited modulation bandwidth of LEDs. The normalized impulse response of the LED is [32]

$$u(t) = \varepsilon e^{-2\pi f_b t}, \quad (6)$$

where f_b is the 3-dB modulation bandwidth of the LED and ε is a normalized coefficient such that $\int (u(t))^2 dt = 1$. The equivalent channel from the l -th LED of the j -th group to the k -th PD is defined as

$$v_{k,(j,l)}(t) = q_{k,(j,l)}(t) \otimes u(t), \quad (7)$$

where \otimes stands for convolution. As the 3-dB bandwidth of the LED is about tens of MHz, the 3-dB bandwidth of the equivalent channel is also tens of MHz. Therefore, the equivalent channel will be frequency selective when the transmission rate is high (hundreds of Mega symbol/s).

III. TRANSMISSION STRATEGY AND PAM CONSTELLATION DESIGN

The block diagram of the proposed bipolar PAM based OSM scheme is shown in Fig. 1. In the proposed bipolar PAM based OSM scheme, $n_t/2$ data streams can be transmitted simultaneously, and only one LED of each group is active at any given time instance. As the bipolar PAM signal cannot be transmitted directly in the IM/DD VLCs, the polarity information of the bipolar PAM signal is mapped to the index of LED in each group, and the absolute value of the bipolar PAM signal is transmitted through the corresponding LED. For example, when the bipolar PAM signal is positive, the absolute value of the signal is transmitted through the first LED of the corresponding group; when the bipolar PAM signal is negative, the absolute value of the signal is transmitted through the second LED of the corresponding group.

In Fig. 1 (a), the un-clipped bipolar signal $x_j(t)$ of the j -th data stream is

$$x_j(t) = \sum_{n=-\infty}^{+\infty} \alpha_j(n)g(t - nT_s), \quad (8)$$

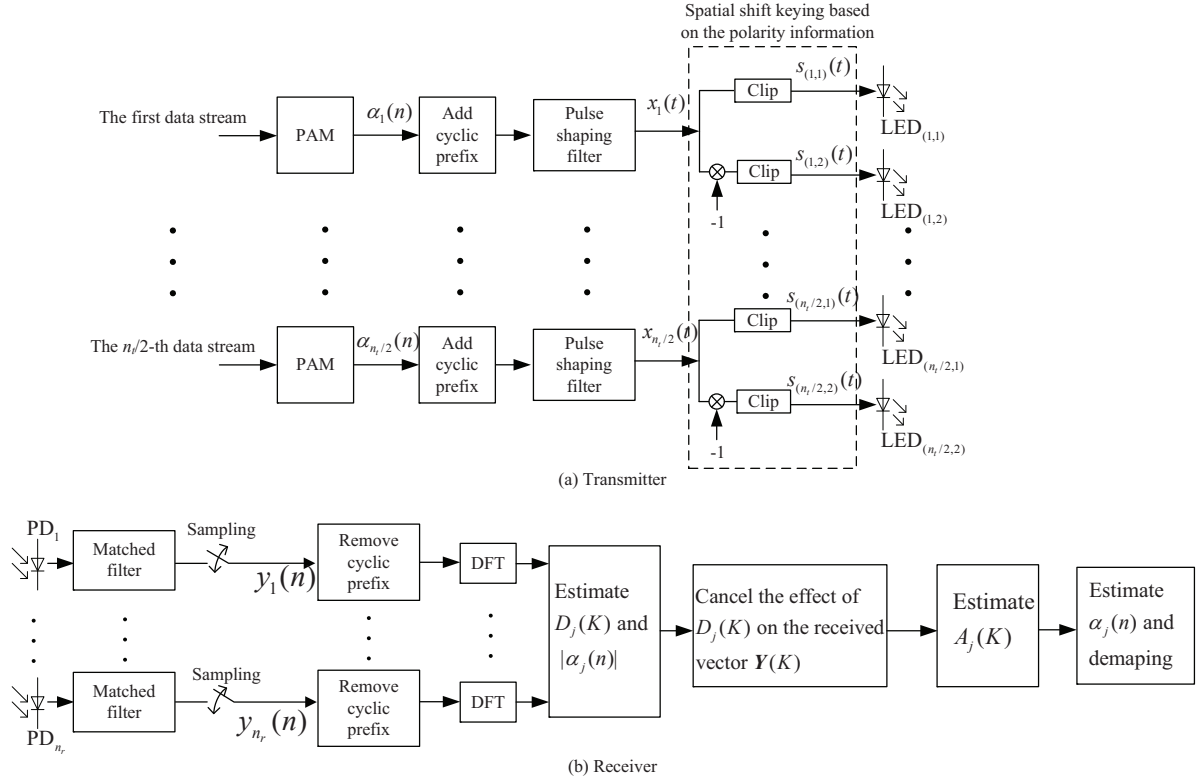


Fig. 1. The block diagram of the proposed PAM based OSM scheme. (a) Transmitter; (b) Receiver.

where $\alpha_j(n)$ is the n -th modulated bipolar PAM symbol, T_s is the symbol interval, $g(t)$ is the impulse response of the pulse-shaping filter and normalized as $\int (g(t))^2 dt = 1$ and a Gaussian pulse-shaping filter is employed [33].

The signal fed to the first LED of the j -th group is expressed as

$$\begin{aligned}
 s_{(j,1)}(t) &= (x_j(t))^+ = (x_j(t) + |x_j(t)|)/2 \\
 &= \sum_{n=-\infty}^{+\infty} (\alpha_j(n))^+ g(t - nT_s) \\
 &= \sum_{n=-\infty}^{+\infty} z_{(j,1)}(n) g(t - nT_s),
 \end{aligned} \tag{9}$$

where $z_{(j,1)}(n) = (\alpha_j(n))^+ = (\alpha_j(n) + |\alpha_j(n)|)/2$, $(a)^+ = \max\{0, a\}$, and a is a real number.

The signal fed to the second LED of the j -th group is expressed as

$$\begin{aligned}
s_{(j,2)}(t) &= (-x_j(t))^+ = (-x_j(t) + |x_j(t)|)/2 \\
&= \sum_{n=-\infty}^{+\infty} (-\alpha_j(n))^+ g(t - nT_s) \\
&= \sum_{n=-\infty}^{+\infty} z_{(j,2)}(n) g(t - nT_s),
\end{aligned} \tag{10}$$

where $z_{(j,2)}(n) = (-\alpha_j(n))^+ = (-\alpha_j(n) + |\alpha_j(n)|)/2$. Through the operations of (9) and (10), the polarity information of the bipolar PAM signal $\alpha_j(n)$ is mapped to the index of LED of the j -th group.

As the original positive signals and negative signals are transmitted by the first and the second LED in each group, respectively, the detection of the polarity is very important for the data recovering in the proposed bipolar PAM based OSM scheme. Therefore, the constellation diagram of PAM is redesigned. Let the minimum distance between two adjacent points in the constellation of the traditional bipolar M -PAM signals be $2d$. With the traditional constellation, the modulated signal $\alpha_{j,\text{traditional}}(n)$ is

$$\begin{aligned}
\alpha_{j,\text{traditional}}(n) \in \{ &(-M + 1)d, (-M + 3)d, \dots, -d, \\
&d, \dots, (M - 3)d, (M - 1)d\}.
\end{aligned} \tag{11}$$

The minimal distance between the positive signals and the negative signals is also $2d$.

In the proposed bipolar PAM based OSM scheme, the modulated signal is redesigned as

$$\alpha_j(n) = \alpha_{j,\text{traditional}}(n) + B \cdot \text{sign}\{\alpha_{j,\text{traditional}}(n)\} \cdot d, \tag{12}$$

where $\text{sign}\{\cdot\}$ is the sign function. The parameter B is introduced to control the distance between the positive signals and the negative signals, and it affects the estimation performance of the polarity information. The constellation of the modified bipolar M -PAM can be expressed as

$$\begin{aligned}
\{ &(-M + 1 - B)d, (-M + 3 - B)d, \dots, (-1 - B)d, \\
&(1 + B)d, \dots, (M - 3 + B)d, (M - 1 + B)d\}.
\end{aligned} \tag{13}$$

It is easy to show that the minimal distance between the positive signals and the negative signals in the redesigned bipolar PAM scheme is $(2 + 2B)d$, while the minimal distance between the adjacent points is still $2d$. Note that under the optical transmission power constraint, d will decrease as B increases, and there is an optimal value of B that minimizes SER.

IV. RECEIVE ALGORITHM OF THE PROPOSED OSM SCHEME

The received signal of the k -th PD in the time domain is

$$r_k(t) = \sum_{j=1}^{n_t/2} \sum_{l=1}^2 s_{(j,l)}(t) \otimes v_{k,(j,l)}(t) + N_k(t), \quad (14)$$

where $N_k(t)$ is the noise component at the k -th PD, and the variance of $N_k(t)$ can be expressed as [6], [34]

$$\sigma_N^2 = \sigma_{\text{shot}}^2 + \sigma_{\text{thermal}}^2, \quad (15)$$

where σ_{shot}^2 is the variance of shot-noise, which is related to the average optical power of ambient light, and $\sigma_{\text{thermal}}^2$ is the variance of thermal-noise. These noises can be accurately modeled as an additive white Gaussian noise (AWGN) [6] [35].

The matched filter is a part of the receiver [36], and the output of the matched filter in the proposed bipolar PAM based OSM scheme is given by

$$\begin{aligned} y_k(t) &= r_k(t) \otimes \beta(t) \\ &= \sum_{j=1}^{n_t/2} \sum_{l=1}^2 s_{(j,l)}(t) \otimes v_{k,(j,l)}(t) \otimes \beta(t) + N_k(t) \otimes \beta(t) \\ &= \sum_{j=1}^{n_t/2} \sum_{l=1}^2 \sum_{n=-\infty}^{+\infty} z_{(j,l)}(n) g(t - nT_s) \otimes v_{k,(j,l)}(t) \otimes \beta(t) + w_k(t) \\ &= \sum_{j=1}^{n_t/2} \sum_{l=1}^2 \sum_{n=-\infty}^{+\infty} z_{(j,l)}(n) \delta(t - nT_s) \otimes h_{k,(j,l)}(t) + w_k(t), \end{aligned} \quad (16)$$

where $\beta(t) = g(T_s - t)$ is the impulse response of the matched filter, $h_{k,(j,l)}(t) = g(t) \otimes v_{k,(j,l)}(t) \otimes \beta(t)$, $w_k(t)$ is the noise component with variance σ_w^2 , and $\sigma_w^2 = \sigma_N^2$. The received signal of the k -th PD at the n -th sampling instance can be expressed as

$$y_k(n) = \sum_{j=1}^{n_t/2} \sum_{l=1}^2 z_{(j,l)}(n) \otimes h_{k,(j,l)}(n) + w_k(n). \quad (17)$$

In the following analysis and derivation, perfect symbol timing in the receiver is assumed. Symbol timing estimation processes developed for RF systems, for example, the early-late gate scheme, can be used in VLCs.

According to (17), after discrete Fourier transform (DFT), which can be implemented by using the fast Fourier transform (FFT) algorithm, the received signal at the K -th frequency point is

written as

$$\mathbf{Y}(K) = \mathbf{C}(K) \begin{bmatrix} Z_{(1,1)}(K) \\ Z_{(1,2)}(K) \\ \vdots \\ Z_{(n_t/2,1)}(K) \\ Z_{(n_t/2,2)}(K) \end{bmatrix} + \mathbf{W}(K), \quad (18)$$

where $\mathbf{Y}(K) = [Y_1(K), \dots, Y_{n_r}(K)]^T$, $Y_k(K) = \text{DFT}\{y_k(n)\}$, and where $\text{DFT}\{\cdot\}$ denotes DFT operation; $\mathbf{C}(K) = [\mathbf{c}_{(1,1)}(K), \dots, \mathbf{c}_{(n_t/2,2)}(K)]$ is the frequency domain channel matrix at the K -th frequency point, $\mathbf{c}_{(j,l)}(K) = [c_{1,(j,l)}(K), \dots, c_{n_r,(j,l)}(K)]^T$, $c_{k,(j,l)}(K) = \text{DFT}\{h_{k,(j,l)}(n)\}$, and $(\cdot)^T$ denotes transpose; $Z_{(j,l)}(K) = \text{DFT}\{z_{(j,l)}(n)\}$; $\mathbf{W}(K)$ is the frequency domain noise component, each element of $\mathbf{W}(K)$ is with variance $\sigma_W^2 = N\sigma_w^2$, $K \in \{0, 1, \dots, N-1\}$, and N is the length of DFT.

A. MMSE FDE receive algorithm

The MMSE FDE receive algorithm is a straightforward scheme to detect the information in the PAM based OSM scheme [28], and it is as a benchmark algorithm for the performance comparison. By applying MMSE FDE algorithm, according to (18), the estimates of $Z_{(j,1)}(K)$ and $Z_{(j,2)}(K)$ can be expressed as [37]

$$\begin{bmatrix} \hat{Z}_{(1,1)}(K) \\ \vdots \\ \hat{Z}_{(n_t/2,2)}(K) \end{bmatrix} = \left(\mathbf{C}(K)^H \mathbf{C}(K) + \frac{\sigma_W^2}{\sigma_{Z(K)}^2} \mathbf{I}_{n_t} \right)^{-1} \mathbf{C}(K)^H \mathbf{Y}(K), \quad (19)$$

where $(\cdot)^H$ stands for conjugate-transpose, \mathbf{I}_{n_t} is an identity matrix with rank n_t , and $\sigma_{Z(K)}^2$ is the variance of $Z_{(j,l)}(K)$. Because $\alpha_j(n) = z_{(j,1)}(n) - z_{(j,2)}(n)$, the estimate of the frequency domain signal of $\alpha_j(n)$, $A_j(K)$, is given by

$$\hat{A}_j(K)_{\text{MMSE}} = \hat{Z}_{(j,1)}(K) - \hat{Z}_{(j,2)}(K), \quad (20)$$

where $A_j(K) = \text{DFT}\{\alpha_j(n)\}$. The estimate of $\alpha_j(n)$ can be derived by transferring $\hat{A}_j(K)_{\text{MMSE}}$ into the time domain as

$$\hat{\alpha}_{j,\text{MMSE}}(n) = \text{IDFT}\{\hat{A}_j(K)_{\text{MMSE}}\}, \quad (21)$$

where $\text{IDFT}\{\cdot\}$ stands for inverse DFT (IDFT) operation.

B. Proposed novel receive algorithm

Although the MMSE FDE receive algorithm is simple and straightforward, the SER performance of the MMSE FDE receive algorithm is not good. Besides, the maximum likelihood receive algorithm is prohibitively complicated and not practical, as ISI exists in the high-rate transmission. Therefore, we propose a novel receive algorithm with the affordable computational complexity, and the proposed receive algorithm achieves good SER performance.

According to (9) and (10), the transmitted signals of the j -th data stream in the frequency domain can be expressed as

$$\begin{cases} Z_{(j,1)}(K) = (A_j(K) + D_j(K))/2 \\ Z_{(j,2)}(K) = (-A_j(K) + D_j(K))/2 \end{cases}, \quad (22)$$

where $D_j(K) = \text{DFT}\{|\alpha_j(n)|\}$. Therefore, Eq. (18) can be rewritten as

$$\begin{aligned} \mathbf{Y}(K) &= \sum_{j=1}^{n_t/2} \frac{\mathbf{c}_{(j,1)}(K) + \mathbf{c}_{(j,2)}(K)}{2} D_j(K) + \frac{\mathbf{c}_{(j,1)}(K) - \mathbf{c}_{(j,2)}(K)}{2} A_j(K) + \mathbf{W}(K) \\ &= \sum_{j=1}^{n_t/2} \tilde{\mathbf{c}}_{(j,1)}(K) D_j(K) + \tilde{\mathbf{c}}_{(j,2)}(K) A_j(K) + \mathbf{W}(K) \\ &= \tilde{\mathbf{C}}_1(K) \mathbf{D}(K) + \tilde{\mathbf{C}}_2(K) \mathbf{A}(K) + \mathbf{W}(K), \end{aligned} \quad (23)$$

where $\tilde{\mathbf{c}}_{(j,1)}(K) = (\mathbf{c}_{(j,1)}(K) + \mathbf{c}_{(j,2)}(K))/2$; $\tilde{\mathbf{c}}_{(j,2)}(K) = (\mathbf{c}_{(j,1)}(K) - \mathbf{c}_{(j,2)}(K))/2$; $\tilde{\mathbf{C}}_1(K) = [\tilde{\mathbf{c}}_{(1,1)}(K), \tilde{\mathbf{c}}_{(2,1)}(K), \dots, \tilde{\mathbf{c}}_{(n_t/2,1)}(K)]$; $\tilde{\mathbf{C}}_2(K) = [\tilde{\mathbf{c}}_{(1,2)}(K), \tilde{\mathbf{c}}_{(2,2)}(K), \dots, \tilde{\mathbf{c}}_{(n_t/2,2)}(K)]$; $\mathbf{A}(K) = [A_1(K), \dots, A_{n_t/2}(K)]^T$; $\mathbf{D}(K) = [D_1(K), \dots, D_{n_t/2}(K)]^T$. Define $\tilde{\mathbf{C}}(K) = [\tilde{\mathbf{C}}_1(K), \tilde{\mathbf{C}}_2(K)]$.

Because $\mathbf{c}_{(j,1)}(K)$ and $\mathbf{c}_{(j,2)}(K)$ are usually correlated in VLCs, the angle between $\mathbf{c}_{(j,1)}(K)$ and $\mathbf{c}_{(j,2)}(K)$ is less than 90 degrees. Thus,

$$\|\mathbf{c}_{(j,1)}(K) - \mathbf{c}_{(j,2)}(K)\|_2^2 < \|\mathbf{c}_{(j,1)}(K) + \mathbf{c}_{(j,2)}(K)\|_2^2. \quad (24)$$

Therefore, we will recover $\mathbf{D}(K)$ first.

By using the linear MMSE criterion, the estimate of $D_j(K)$ ($j = 1, \dots, n_t/2$) is expressed as [38]

$$\hat{D}_j(K) = \frac{\tilde{\mathbf{c}}_{(j,1)}(K)^H \mathbf{R}_j(K)^{-1}}{\tilde{\mathbf{c}}_{(j,1)}(K)^H \mathbf{R}_j(K)^{-1} \tilde{\mathbf{c}}_{(j,1)}(K)} \mathbf{Y}(K) \quad (25)$$

where $\mathbf{R}_j(K)$ is a covariance matrix and is given by

$$\mathbf{R}_j(K) = \sigma_W^2 \mathbf{I}_{n_r} + \sum_{i=1, i \neq j}^{n_t/2} \tilde{\mathbf{c}}_{(i,1)}(K) \tilde{\mathbf{c}}_{(i,1)}(K)^H \sigma_{D(K)}^2 + \sum_{i=1}^{n_t/2} \tilde{\mathbf{c}}_{(i,1)}(K) \tilde{\mathbf{c}}_{(i,1)}(K)^H \sigma_{A(K)}^2, \quad (26)$$

where $\sigma_{A(K)}^2 = E[A_j(K)^* A_j(K)]$, $\sigma_{D(K)}^2 = E[D_j(K)^* D_j(K)]$, and where $(\cdot)^*$ denotes conjugate operation.

We detect $|\alpha_j(n)|$ by transferring $\hat{D}_j(K)$ into the time domain. Because $|\alpha_j(n)|$ is the absolute value of an M -PAM constellation point, $|\widehat{\alpha_j(n)}|$ is quantized to the nearest constellation point of M -PAM, which is denoted by $m_j(n)$. The estimate of $D_j(K)$ is updated by transferring $m_j(n)$ into the frequency domain, and the updated estimate of $D_j(K)$ is denoted by $\tilde{D}_j(K)$. Assuming $D(K)$ is correctly estimated, we define a new vector $\mathbf{P}(K)$ as

$$\begin{aligned} \mathbf{P}(K) &= \mathbf{Y}(K) - \tilde{\mathbf{C}}_1(K) \tilde{\mathbf{D}}(K) \\ &= \tilde{\mathbf{C}}_2(K) \mathbf{A}(K) + \mathbf{W}(K), \end{aligned} \quad (27)$$

where $\tilde{\mathbf{D}}(K) = [\tilde{D}_1(K), \dots, \tilde{D}_{n_t/2}(K)]^T$.

The estimate of $\mathbf{A}(K)$ can be derived according to the MMSE criterion as

$$\hat{\mathbf{A}}(K) = \left(\tilde{\mathbf{C}}_2(K)^H \tilde{\mathbf{C}}_2(K) + \frac{\sigma_W^2}{\sigma_{A(K)}^2} \mathbf{I}_{n_t/2} \right)^{-1} \tilde{\mathbf{C}}_2(K)^H \mathbf{P}(K), \quad (28)$$

where $\hat{\mathbf{A}}(K) = [\hat{A}_1(K), \dots, \hat{A}_{n_t/2}(K)]^T$.

After IDFT, the sign of $\alpha_j(n)$ can be estimated as

$$\text{sg}_j(n) = \text{sign}\{\text{IDFT}\{\hat{A}_j(K)\}\}. \quad (29)$$

Therefore, the estimate of $\alpha_j(n)$ is

$$\hat{\alpha}_j(n) = \text{sg}_j(n) \cdot |\widehat{\alpha_j(n)}|. \quad (30)$$

The proposed receive algorithm for the bipolar PAM based OSM scheme is summarized in Table I (Algorithm 1).

The achieved data rate of the proposed bipolar PAM based OSM scheme is

$$R_{\text{OSM}} = \sum_{j=1}^{n_t/2} \frac{N}{N + N_g} \log_2(M_{j,\text{OSM}}) \quad (\text{bits/s/Hz}), \quad (31)$$

where N_g is the length of cyclic prefix, and $M_{j,\text{OSM}}$ is the PAM modulation order of the j -th data stream.

TABLE I
ALGORITHM 1

Step 1:	Estimate $D_j(K)$ ($j = 1, \dots, n_t/2$) by employing the linear MMSE algorithm
Step 2:	Derive the estimate of $ \alpha_j(n) $ by transferring $\hat{D}_j(K)$ into time domain, and the estimate of $ \alpha_j(n) $ is denoted by $ \widehat{\alpha_j(n)} $
Step 3:	Quantize $ \widehat{\alpha_j(n)} $ to the nearest M -PAM constellation point $m_j(n)$
Step 4:	Transfer $m_j(n)$ into the frequency domain, and update the estimate of $D_j(K)$
Step 5:	Cancel the effect of $\mathbf{D}(K)$ on the received vector $\mathbf{Y}(K)$
Step 6:	Employ the linear MMSE algorithm in the frequency domain to estimate $A_j(K)$
Step 7:	Estimate the sign of $\alpha_j(n)$ by transferring the estimate of $A_j(K)$ into time domain, and the estimated the sign of $\alpha_j(n)$ is denoted by $\text{sg}_j(n)$
Step 8:	Derive the estimate of $\alpha_j(n)$ according to $ \widehat{\alpha_j(n)} $ and $\text{sg}_j(n)$
Step 9:	PAM demodulation

C. SER performance of the proposed receive algorithm

In this subsection, we analyze the SER of the proposed receive algorithm. As the estimate of $\alpha_j(n)$ is derived according to $|\widehat{\alpha_j(n)}|$ and $\text{sg}_j(n)$, the estimation performances of $|\alpha_j(n)|$ and the polarity information are analyzed in detail. The analytical expression of SER lower bound is derived for the proposed receive algorithm. Besides, based on the derived SER lower bound, the suboptimal B can be calculated numerically.

The output electrical signal-to-noise ratio (eSNR) of $D_j(K)$ in the proposed receive algorithm can be expressed as [38]

$$\text{SNR}_{D_j(K)} = \tilde{\mathbf{c}}_{(j,1)}(K)^H \mathbf{R}_j(K)^{-1} \tilde{\mathbf{c}}_{(j,1)}(K) \sigma_{D(K)}^2, \quad (32)$$

The statistical properties of $A_j(K)$ and $D_j(K)$ are derived in Appendix A. The output eSNR of

$|\alpha_j(n)|$ is

$$\text{SNR}_{|\alpha_j(n)|} = \frac{\sigma_\alpha^2}{\frac{1}{N^2} \sum_{K=0}^{N-1} \frac{\sigma_{D(K)}^2}{\text{SNR}_{D_j(K)}}}, \quad (33)$$

where $E[|\alpha_j(n)|^2] = E[\alpha_j(n)^2] = \sigma_\alpha^2$ denotes the electrical power of $|\alpha_j(n)|$ and $E[\cdot]$ stands for the expectation of a random variable. The modulation scheme of $|\alpha_j(n)|$ is equivalent to $M/2$ -PAM, as there are only $M/2$ constellation points for $|\alpha_j(n)|$. The minimum Euclidean distance between the adjacent constellation points is

$$d_{\min,|\alpha_j|} = 2\sqrt{\frac{3M\sigma_\alpha^2}{(M+B_j)((M+B_j)^2-1)}}. \quad (34)$$

where B_j is the value of parameter B for the j -th data stream.

Therefore, the SER of $|\alpha_j(n)|$ can be calculated as [36]

$$\begin{aligned} \text{Ps}_{|\alpha_j(n)|} &= \frac{2(M/2-1)}{M/2} Q\left(\frac{d_{\min,|\alpha|}/2}{\sigma_{\text{noise}}}\right) \\ &= \frac{2(M/2-1)}{M/2} Q\left(\sqrt{\frac{3M\text{SNR}_{|\alpha_j(n)|}}{(M+B_j)((M+B_j)^2-1)}}\right), \end{aligned} \quad (35)$$

where $Q(\cdot)$ is the Q -function.

If $D(K)$ is correctly estimated, the eSNR with respect to $A_j(K)$ in (28) is written as [37]

$$\text{SNR}_{A_j(K)} = \frac{\sigma_{A(K)}^2/\sigma_W^2}{\left[\left(\mathbf{C}_2(K)^H \mathbf{C}_2(K) + \frac{\sigma_W^2}{\sigma_{A(K)}^2} \mathbf{I}_{n_t/2}\right)^{-1}\right]_{j,j}} - 1, \quad (36)$$

where $[\cdot]_{j,j}$ is the j -th diagonal element of a matrix. After IDFT, the eSNR of $\alpha_j(n)$ is

$$\text{SNR}_{\alpha_j(n)} = \frac{1}{\frac{1}{N} \sum_{K=0}^{N-1} \frac{1}{\text{SNR}_{A_j(K)}}}. \quad (37)$$

Therefore, if all $|\alpha_j(n)|$ ($n = 0, 1, \dots, N-1$) are estimated correctly, the error probability of $\text{sg}_j(n)$ is expressed as

$$\text{Ps}_{\text{sg}_j(n)|\alpha_j(n)} = \frac{2}{M} \sum_{i=1}^{M/2} Q\left((2i-1+B_j)\sqrt{\frac{3M\text{SNR}_{\alpha_j(n)}}{(M+B_j)((M+B_j)^2-1)}}\right). \quad (38)$$

In the proposed receive algorithm, the estimate of $\alpha_j(n)$ is derived based on $|\widehat{\alpha_j(n)}|$ and $\text{sg}_j(n)$, that is, the estimate of $\alpha_j(n)$ is correct if and only if $|\widehat{\alpha_j(n)}|$ and $\text{sg}_j(n)$ are estimated

correctly. Therefore, when employing the proposed receive algorithm, the SER performance of the j -th data stream is

$$\text{SER}_j = 1 - (1 - \text{Ps}_{|\alpha_j(n)|})(1 - \text{Ps}_{\text{sg}_j(n)}) \quad (39)$$

where $\text{Ps}_{\text{sg}_j(n)}$ is the error rate of $\text{sg}_j(n)$. Note that

$$\text{Ps}_{\text{sg}_j(n)} \geq \text{Ps}_{\text{sg}_j(n)||\alpha_j(n)}. \quad (40)$$

Because the detection and interference cancellation is applied in the estimation of the polarity information $\text{sg}_j(n)$, the estimation performance of $\text{sg}_j(n)$ is relied on the estimates of $|\alpha_j(n)|$. When some of $|\alpha_j(n)|$ are incorrectly estimated, the derivation of the error rate of $\text{sg}_j(n)$ is prohibitively complicated that is the analytical expression of $\text{Ps}_{\text{sg}_j(n)}$ is difficult to be derived. Therefore, we derive the SER lower bound of the proposed receive algorithm as

$$\text{SER}_j \geq 1 - (1 - \text{Ps}_{|\alpha_j(n)|})(1 - \text{Ps}_{\text{sg}_j(n)||\alpha_j(n)}). \quad (41)$$

When the transmit power is normalized, there is an optimal B_j that minimizes the SER of the proposed scheme, that is, the optimal B_j should satisfy

$$B_{\text{optimal},j} = \arg \min_{B_j} \{\text{SER}_j\} \quad (42)$$

However, it is challenging to derive the analytical expression of the optimal B_j , as the exact SER expression is hard to be derived. It can be seen from (41) that the lower bound SER is dominated by the maximum one of $\text{Ps}_{|\alpha_j(n)|}$ and $\text{Ps}_{\text{sg}_j(n)||\alpha_j(n)}$. We derive a suboptimal value of B_j , and the suboptimal value of B_j is designed such that

$$\text{Ps}_{|\alpha_j(n)|} = \text{Ps}_{\text{sg}_j(n)||\alpha_j(n)}. \quad (43)$$

The suboptimal value of B can be derived numerically.

D. Complexity Analysis

In the high-rate IM/DD VLCs, DCO-OFDM or ACO-OFDM based OSM can be applied to combat ISI [18]. In the complexity analysis, we will take DCO-OFDM based OSM as an example. For fair comparison, it is assumed that there are also $n_t/2$ data streams transmitted in the DCO-OFDM based OSM scheme. Therefore, in each modulated subcarrier, the computational complexity is $\mathcal{O}(M^{n_t/2})$ when the ML detector is applied. In DCO-OFDM, the number of modulated subcarriers is $N/2-1$. Besides, the DCO-OFDM based OSM involves $n_t/2$ IDFT operations

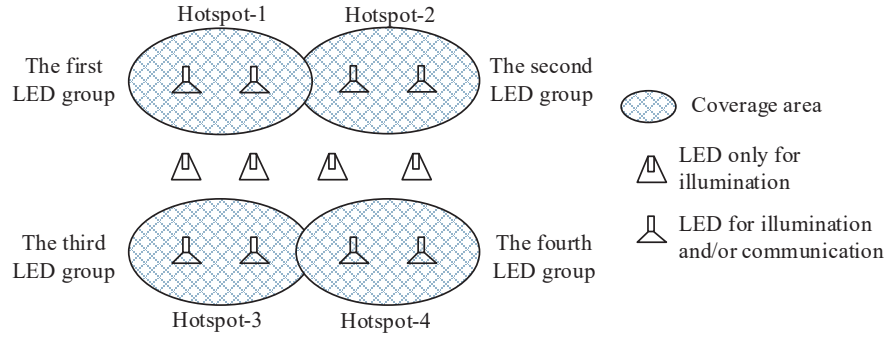


Fig. 2. Coverage area of different LED groups.

at the transmitter and n_r DFT operations at the receiver. Therefore, the computational complexity of the DCO-OFDM based OSM is $\mathcal{O}((N/2 - 1)M^{n_t/2}) + \mathcal{O}((n_t/2 + n_r)N \log_2(N))$.

For the MMSE FDE receive algorithm, the computational complexity of (19) is $\mathcal{O}(n_t^3)$. The signals are Hermitian symmetric in the frequency domain. The computational complexity of the linear MMSE algorithm in the frequency domain is $\mathcal{O}((N/2 - 1)n_t^3)$. In addition, the MMSE FDE receive algorithm involves n_r DFT and $n_t/2$ IDFT operations. Therefore, the computational complexity of the MMSE FDE receive algorithm is $\mathcal{O}((N/2 - 1)n_t^3) + \mathcal{O}((n_t/2 + n_r)N \log_2(N))$.

For the proposed receive algorithm, the computational complexity of (25) is $\mathcal{O}(n_t^3)$; the computational complexity of (28) is $\mathcal{O}((n_t/2)^3)$. The proposed receive algorithm involves $(n_r + n_t/2)$ DFT and n_t IDFT operations. Therefore, the computational complexity of the proposed receive algorithm is $\mathcal{O}((N/2 - 1)n_t^3) + \mathcal{O}((n_r + 3n_t/2)N \log_2(N))$. It is concluded that the computational complexity of the proposed receive algorithm will be much lower than that of the ML detector for the DCO-OFDM based OSM, when the modulation order M increases.

V. PROPOSED SPATIAL AREA DIVISION STRATEGY

The factors including the positions, orientations, and physical parameters of LEDs and PDs govern the correlation of spatial subchannels. The spatial subchannels are highly correlated that is the condition number of the channel matrix is much greater than one. When the spatial subchannels of MIMO VLC systems are highly correlated, the system performance of the proposed OSM scheme with multiple independent data streams will be degraded. In this case, we can deploy the LEDs carefully such that each group of LEDs is responsible for a specific

area, and the coverage areas of different LED groups are partially overlapped with each other. In the overlapped area, the proposed receive algorithm in Section IV.B can be applied. In the non-overlapped area, the receiver only receives the signal from one LED group. In this section, we focus on analyzing the receive algorithm for the non-overlapped coverage area.

The illustration of the coverage areas of different LED groups is shown in Fig. 2. In the central area of one hotspot, there is only one LED group covering this area, and the channel correlation of different LED groups is reduced. For example, when a user is in the central covering area of the j -th LED group, the received signal of the k -th PD of the user can be expressed as

$$r_{j,k}(t) = \sum_{l=1}^2 s_{(j,l)}(t) \otimes v_{k,(j,l)}(t) + N_{j,k}(t), \quad (44)$$

where $N_{j,k}(t)$ is the noise component.

After passing through the match filter $\beta(t)$, the received signal of the k -th PD at the n -th sampling instance can be expressed as

$$y_{j,k}(n) = \sum_{l=1}^2 z_{(j,l)}(n) \otimes h_{k,(j,l)}(n) + w_{j,k}(n). \quad (45)$$

where $w_{j,k}(t) = N_{j,k}(t) \otimes \beta(t)$.

In the frequency domain, the received signal at the K -th frequency point is written as

$$\mathbf{Y}_j(K) = [\mathbf{c}_{(j,1)}(K), \mathbf{c}_{(j,2)}(K)] \begin{bmatrix} Z_{(j,1)}(K) \\ Z_{(j,2)}(K) \end{bmatrix} + \mathbf{W}_j(K), \quad (46)$$

where $\mathbf{Y}_j(K) = [Y_{j,1}(K), \dots, Y_{j,n_r}(K)]^T$, $Y_{j,k}(K) = \text{DFT}\{y_{j,k}(n)\}$, and $\mathbf{W}_j(K)$ is the frequency domain noise component.

According to (23), the frequency domain signal can be rewritten as

$$\mathbf{Y}_j(K) = \tilde{\mathbf{c}}_{(j,1)}(K) D_j(K) + \tilde{\mathbf{c}}_{(j,2)}(K) A_j(K) + \mathbf{W}_j(K). \quad (47)$$

Therefore, the proposed novel receive algorithm can be applied, and detection procedure is same as that in Table I. Note that a user clustering strategy was investigated in [39]. The purpose of user clustering in [39] is to mitigate the intercell interference and improve the cell edge users' performance. Different from [39], the purpose of the proposed spatial division strategy is to reduce the effect of the high correlation of spatial subchannels and improve the performance of the proposed bipolar PAM based OSM scheme.

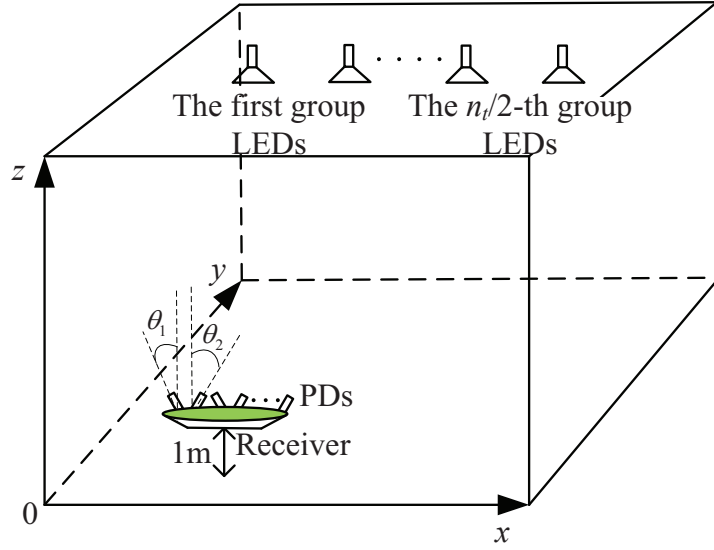


Fig. 3. Indoor $n_t \times n_r$ MIMO VLC model.

TABLE II
SYSTEM PARAMETERS

Semiangle at half power	60 deg
FOV at receiver	60 deg
Detector area	1.0 cm^2
Optical filter gain	0.33
Refractive index of optical concentrator	1.5
Photodiode responsivity	0.7
Walls average reflectivity ρ	0.43

VI. PERFORMANCE EVALUATION

In the simulation, the configuration of the system is shown in Fig. 3, where multiple transmit LEDs and multiple receive PDs are equipped at the transmitter and receiver, respectively. To reduce the correlation of spatial subchannels, the PDs are not put towards the roof, but with an angle in the $(x-z)$ plane as illustrated in Fig. 3. The odd-indexed PDs have an angle of θ_1 and the even-indexed PDs have an angle of θ_2 . Other system parameters are given in Table II. It is assumed that all LEDs and all PDs have the same property, respectively. In the simulation, SNR

is defined according to the optical transmission power as [6]

$$\text{SNR} = \frac{p_t}{\sigma_N}, \quad (48)$$

where $p_t = \sum_{j=1}^{n_t/2} \sum_{l=1}^2 E[s_{(j,l)}(t)]$ is the average optical transmission power.

In the simulation, the 3-dB bandwidth of the equivalent channel is set at 10 MHz, while the used modulated signal bandwidth is 100 MHz, which means that the PAM symbol rate is 100 Mega symbol/s. Therefore, the equivalent channel will be frequency selective and ISI exists in this system. The delay spread of the indoor optical wireless channel is usually in the range of tens of nano-seconds [6], and it is assumed that the delay spread of the equivalent channel is less than 80 ns. In the simulation, both the LOS component and the diffuse component of the channel are considered. The LOS component is calculated according to the positions of LEDs and PDs, the parameters given in the Table II, and (2). The diffuse component is calculated according to (4) and (5), the 3-dB bandwidth, and the parameters given in Table II. The length of cyclic prefix is set to be 8 in the proposed scheme, and the length of cyclic prefix is greater than the delay spread of the equivalent channel. The size of DFT is $N = 1024$.

First, we evaluate the system performance when $n_t = n_r = 2$, that is, two LEDs and two PDs are equipped at the transmitter and the receiver, respectively. The coordinates of the LEDs are (1.5, 3, 6) and (4.5, 3, 6), respectively. Fig. 4 shows the SER performance of the proposed bipolar PAM based OSM scheme, where the two PDs are located at (2.5, 3, 1) and (2.6, 3, 1), respectively, and $\theta_1 = \theta_2 = \pi/8$.

As expected, the SER performance of 16-PAM is better than that of 64-PAM, and 64-PAM is better than 256-PAM. The analytical lower bounds match the simulation results very well. The estimation of $\alpha_j(n)$ in the proposed receive algorithm is related to $|\widehat{\alpha_j(n)}|$ and $\text{sg}_j(n)$. It can be seen from Fig. 4 that as B_j increases from 0 to 2, the SER performance improves significantly at $\text{SER} = 10^{-3}$, which means that when $B_j = 0$, $\text{sg}_j(n)$ dominates the SER in the high-SNR region. As B_j increases, the estimation performance of $\text{sg}_j(n)$ improves, resulting in an improved SER performance of the proposed bipolar PAM based OSM scheme. When $B_j = 0$, the square and triangular curves in Fig. 4 (a) show a deviation behavior, because $\text{sg}_j(n)$ dominates the SER in the middle of the simulated SNR region. The achieved data rates with 16-PAM, 64-PAM, and 256-PAM based proposed schemes are 400 Mbps, 600 Mbps, and 800 Mbps, respectively.

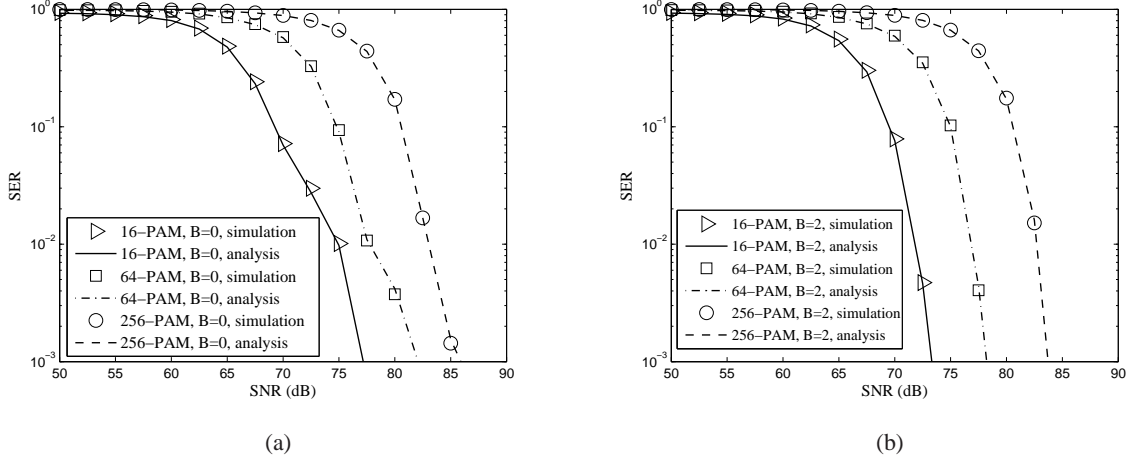


Fig. 4. SER performance of the proposed PAM based OSM scheme (the coordinates of the two LEDs are (1.5, 3, 6) and (4.5, 3, 6), respectively; two PDs are located at (2.5, 3, 1) and (2.6, 3, 1), respectively), and $\theta_1 = \theta_2 = \pi/8$. (a) $B = 0$; (b) $B = 2$.

Note that for a specific modulation order, there is an optimal value of B to minimize the SER under the SNR constraint. However, it is very difficult to analytically derive the optimal value of B . To further characterize the effect of the parameter B to the system performance, Fig. 5 shows the simulated SER of the proposed scheme versus the parameter B . It can be seen from Fig. 5 that the optimal value of B depends on the SNR, the modulation order, and the channel environment. Besides, the analytical results of the SER of $|\alpha_j(n)|$ and the error probability of $sg_j(n)$ are plotted in Fig. 5. When the value of B increases, the SER of $|\alpha_j(n)|$ increases, and the error probability of $sg_j(n)$ decreases. That is because when the transmission power is normalized and the value of B increases, the minimum Euclidean distance between the positive signals and the negative signals increases, but the minimum Euclidean distance between the adjacent points of the redesigned bipolar PAM decreases. It can be seen from Fig. 5 that the suboptimal value of B , which makes (35) and (38) equal, is approximately equal to the optimal value of B . Note that the optimal value of B is to minimize the SER, and the suboptimal value of B is designed such that (35) and (38) equal. For simplicity, when the proposed scheme is employed in the following evaluations, we set B equal to 2.

In Fig. 6, six schemes are employed for BER comparison. By using the proposed transmission strategy, where bipolar 16-PAM is employed, the proposed receive algorithm and the MMSE FDE receive algorithm are carried out, respectively. The third scheme is the 128-ary quadrature

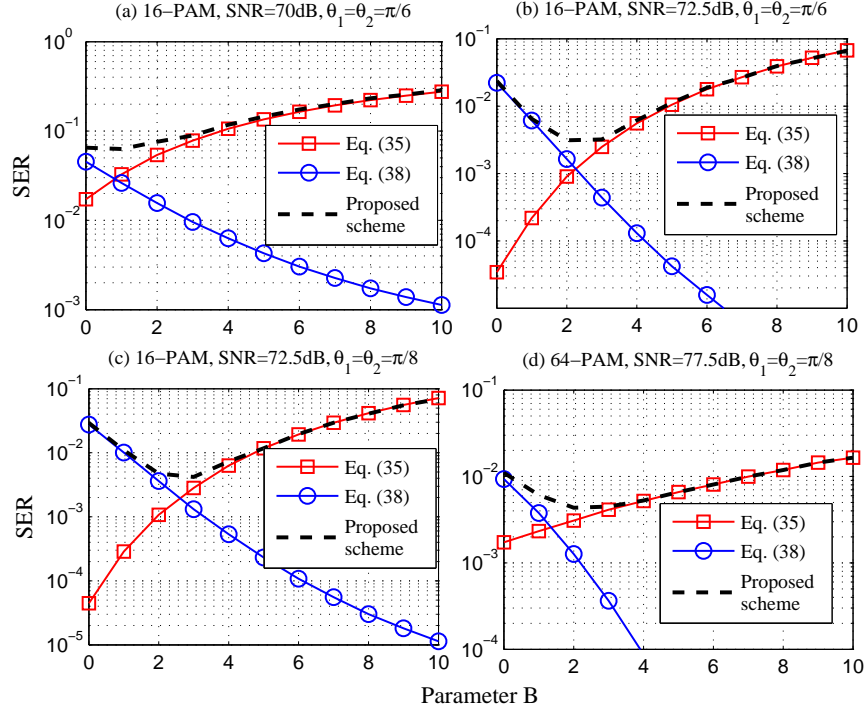


Fig. 5. SER versus the parameter B in different setups.

amplitude modulation (QAM) DCO-OFDM based OSM scheme with an optimal detector (ML detector), where 1 bit information is mapped to the index of LED and 128-QAM is employed at each modulated subcarrier. The unipolar 4-PAM MIMO scheme with FDE is the fourth scheme. The fifth scheme is the unipolar 16-PAM diversity scheme with FDE. The sixth scheme is the 256-QAM flip-OFDM 2×2 MIMO scheme. In the flip-OFDM 2×2 MIMO scheme and the unipolar 4-PAM MIMO scheme scheme, two independent data streams are transmitted through two LEDs, and a linear MMSE receiver is applied in the frequency domain.

The achieved data rate of the DCO-OFDM based OSM scheme is [18], [40]

$$R_{\text{DCO-OFDM OSM}} = \frac{N/2 - 1}{N} \{ \log_2(M_{\text{DCO}}) + \log_2(n_t) \} \quad (\text{bits/s/Hz}), \quad (49)$$

where M_{DCO} is the modulation order of each modulated subcarrier in the DCO-OFDM based OSM scheme.

The achieved data rate of the flip-OFDM based 2×2 MIMO system is [13]

$$R_{\text{flip-OFDM}} = \frac{1}{2} \log_2(M_{\text{flip}}) \quad (\text{bits/s/Hz}), \quad (50)$$

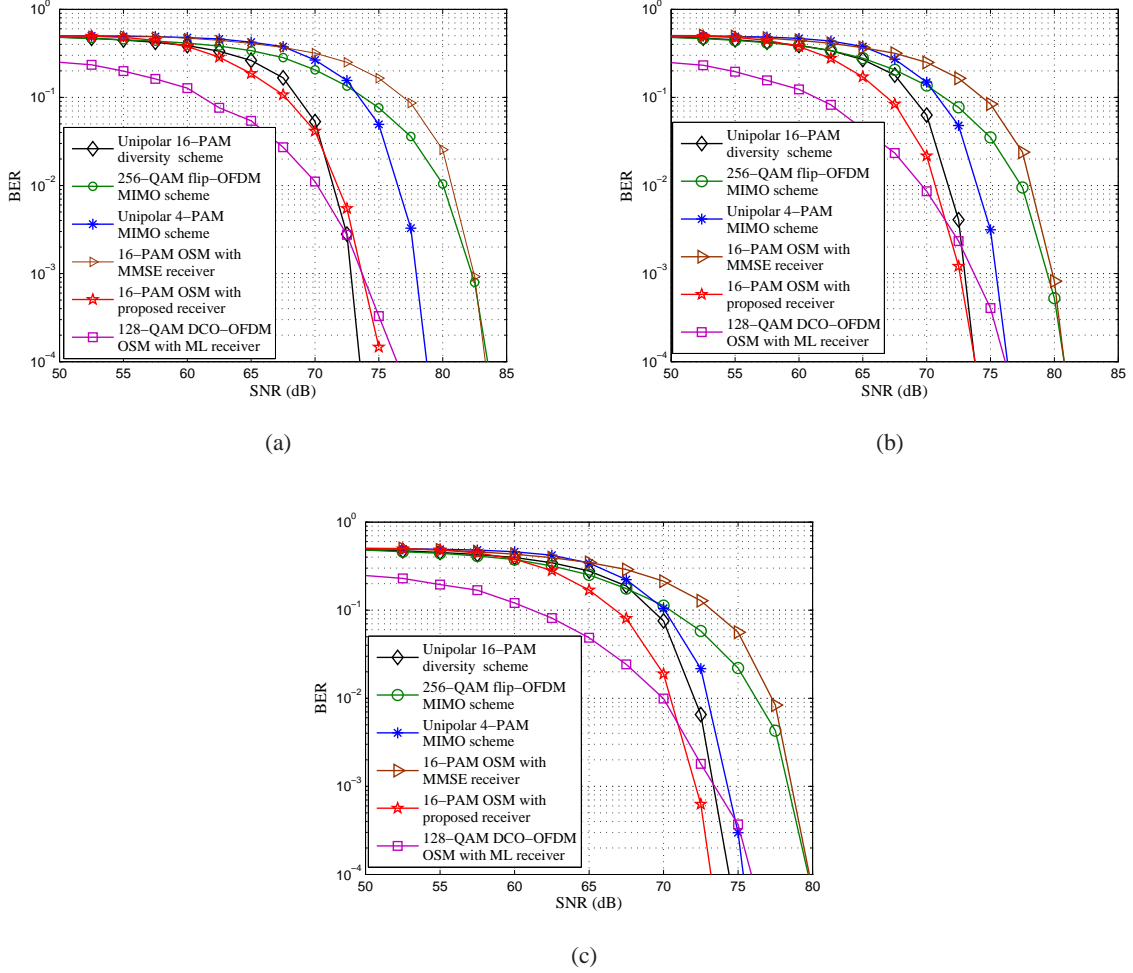


Fig. 6. BER comparison among different schemes (the coordinates of the two LEDs are (1.5, 3, 6) and (4.5, 3, 6), respectively; two PDs are located at (2.5,3,1) and (2.6,3,1), respectively). (a) $\theta_1 = \theta_2 = \pi/16$; (b) $\theta_1 = \theta_2 = \pi/8$; (c) $\theta_1 = \theta_2 = \pi/6$.

where M_{flip} is the modulation order of each modulated subcarrier in the flip-OFDM 2×2 MIMO system. To maintain the same achieved data rates, the modulation orders of the six systems must satisfy the following relationship:

$$\begin{aligned}
 \log_2(M_{\text{OSM}}) &= \log_2(M_{\text{DC-Diversity}}) = 2 \log_2(M_{\text{DC-MIMO}}) \\
 &= \frac{1}{2} \log_2(M_{\text{flip}}) = \frac{1}{2} (\log_2(M_{\text{DCO}}) + 1)
 \end{aligned} \tag{51}$$

where $M_{\text{DC-Diversity}}$ and $M_{\text{DC-MIMO}}$ are the modulation orders of the unipolar PAM diversity scheme and the unipolar PAM MIMO scheme, respectively.

In Fig. 6, all the six schemes achieve the same data rate, and $B = 2$ is employed in the proposed

scheme. It is observed from Fig. 6 (a) that when the correlation between the spatial subchannels is high ($\theta_1 = \theta_2 = \pi/16$), the BER performance of proposed scheme is better than those of the unipolar PAM MIMO scheme and the flip-OFDM based MIMO scheme, while the DCO-OFDM based OSM scheme achieves the best BER performance when $\text{SNR} < 72.5\text{dB}$, and the unipolar PAM diversity scheme achieves the best BER performance when $\text{SNR} > 72.5\text{dB}$. That is because the spatial subchannels are highly correlated and the degree of freedom of the MIMO channel is approximately equal to one. When the correlation becomes low ($\theta_1 = \theta_2 = \pi/8$ as shown in Fig. 6 (b)), the proposed scheme achieves the best BER performance when $\text{SNR} > 72.5\text{dB}$. Under a lower correlation condition of $\theta_1 = \theta_2 = \pi/6$ as shown in Fig. 6 (c), the proposed scheme achieves the best BER performance when $\text{SNR} > 72.5\text{dB}$, and the SNR gain increases. It can be seen from Fig. 6 (c) that the proposed scheme requires the lowest transmit power at $\text{BER} = 10^{-4}$. When compared with the unipolar 4-PAM 2×2 MIMO scheme, the proposed 16-PAM based OSM scheme gains about 2 dB at $\text{BER} = 10^{-4}$. With the same BER target, the proposed scheme gains about 7 dB over the 256-QAM based flip-OFDM 2×2 MIMO scheme. Compared with the unipolar 16-PAM diversity scheme and the 16-PAM based OSM with a MMSE based detector, the proposed scheme gains about 1.5dB and 7 dB, respectively. Besides, when compared with the 128-QAM DCO-OFDM based OSM with an optimal detector, the proposed scheme gains about 3 dB, and has a lower computational complexity when the modulation order increases.

In general, the unipolar diversity scheme achieves the best performance in the high SNR region (required to achieve a practical BER value), when the spatial subchannels are highly correlated. The proposed scheme achieves better performance than other schemes in high SNR region (required to achieve a practical BER value), when the correlation between the spatial subchannels is moderate to low.

PAPR is the ratio between the maximum power and the average power of the transmit signal, that is,

$$\text{PAPR}\{s_{(j,l)}(t)\} = \frac{\max\{|s_{(j,l)}(t)|^2\}}{E[|s_{(j,l)}(t)|^2]}. \quad (52)$$

The complementary cumulative distribution function (CCDF) of $\text{PAPR}\{s_{(j,l)}(t)\}$ is defined as

$$F_{\text{PAPR}}(\text{Th}) = \text{Pr}(\text{PAPR}\{s_{(j,l)}(t)\} > \text{Th}) \quad (53)$$

where $\text{Pr}(\cdot)$ is the probability function.

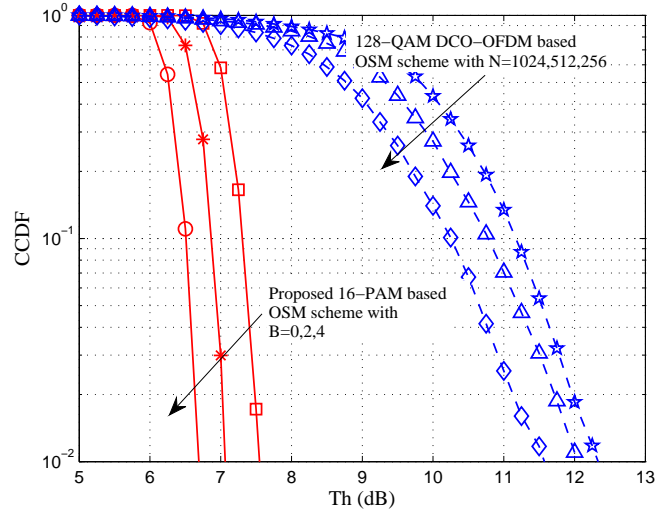


Fig. 7. The CCDFs of the proposed bipolar PAM based OSM scheme and the DCO-OFDM based OSM scheme.

It can be seen from Fig. 7 that when the same data rate is achieved, the PAPR of the proposed bipolar PAM based OSM scheme is much lower than that of the DCO-OFDM based OSM scheme. The PAPR of the proposed bipolar PAM based OSM decreases, when B increases. The PAPR of the DCO-OFDM based OSM increases, when the IDFT size N increases. **PAPR is related to instantaneous envelopes. When the instantaneous envelope has large fluctuations, the PAPR of the signal will be high. When the instantaneous envelope has small fluctuations, the PAPR of the signal will be low.** The instantaneous envelopes of the modulated signals are as shown in Fig. 8, where the peak magnitudes have been normalized to one. The instantaneous envelopes in Fig. 8 confirm the conclusion that the PAPR of the proposed bipolar PAM based OSM scheme is much lower than that of the DCO-OFDM based OSM scheme.

Fig. 9 shows the BER of the proposed scheme when the receiver is placed around, where $\text{SNR} = 75\text{dB}$, $B = 2$, $\theta_1 = \theta_2 = \pi/8$, $M_{\text{OSM}} = 16$, the two PDs are parallel to the x-axis, and the receiver is placed horizontally in the room at a height of 1 m above the ground. It can be seen from Fig. 9 that the BER is below 10^{-4} in all places of the room.

When four LEDs and four PDs are employed, the SER performance of the proposed bipolar PAM based OSM scheme is shown in Fig. 10, where $\theta_1 = \theta_2 = \pi/8$. The four LEDs are located at (0.6, 3, 6), (1.0, 3, 6), (5.0, 3, 6), and (5.4, 3, 6), respectively. The first and the

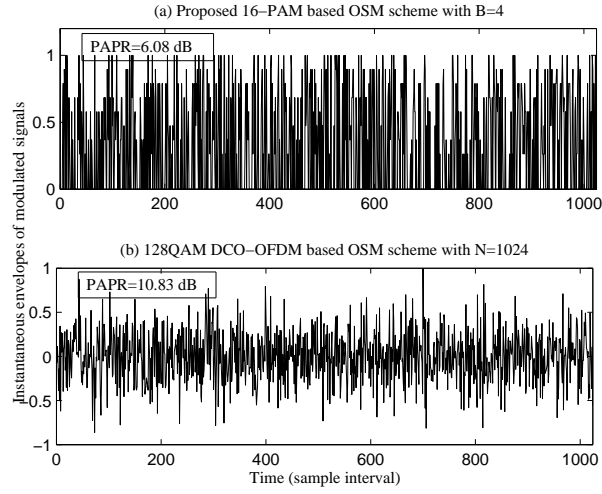


Fig. 8. The instantaneous envelopes of different modulated signals.

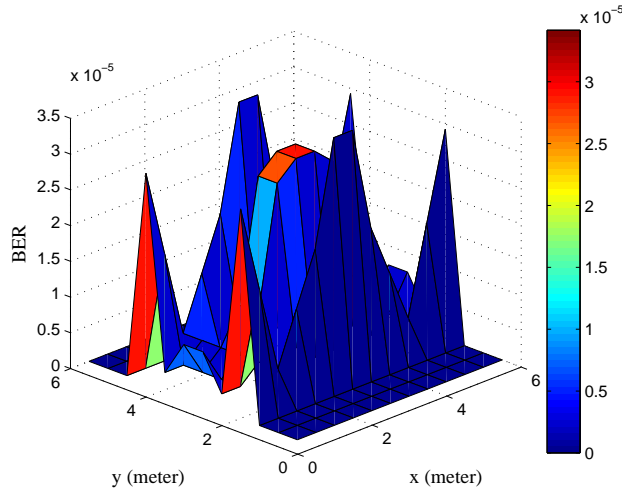


Fig. 9. BER of the proposed PAM based OSM scheme when the receiver is placed around the room. $\text{SNR}=75\text{dB}$, $M_{\text{OSM}}=16$, $B = 2$, $\theta_1 = \theta_2 = \pi/8$, the two PDs are parallel to the x-axis, and the receiver is placed horizontally in the room at height of 1 meter above ground.

second LEDs are in the first group, and the third and the fourth LEDs are in the second group. The coordinates of the four PDs are (2.5,3,1), (2.6,3,1), (2.7,3,1) and (2.8,3,1), respectively. The same conclusion can be drawn as in Fig. 4 that low order modulation outperforms high order modulation. Fig. 10 (a) shows the SER performance of the proposed scheme when two

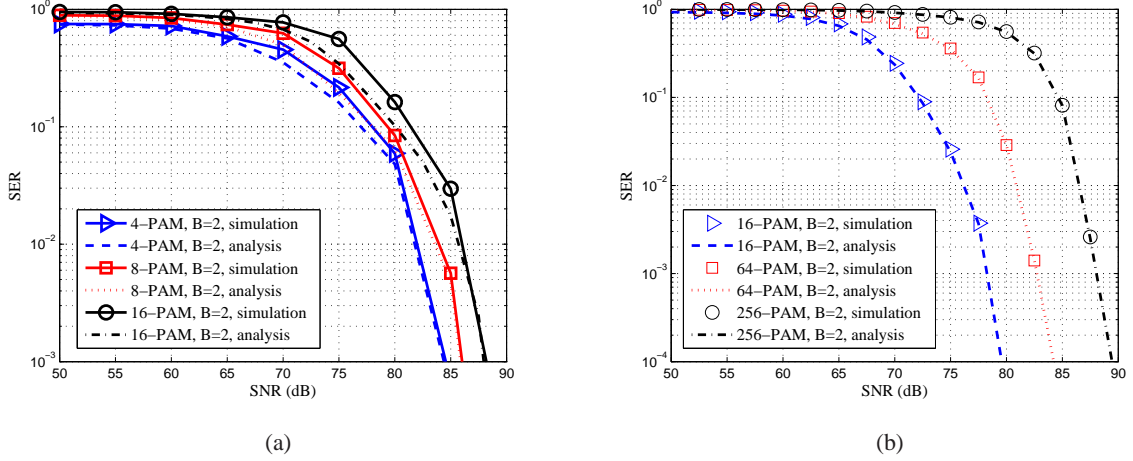



Fig. 10. SER of the proposed PAM based OSM scheme with $n_r = 4$ PDs and $\theta_1 = \theta_2 = \pi/8$. (a) Two data streams, and $n_t = 4$; (b) Proposed spatial area division strategy, and $n_t = 2$.

data streams are transmitted. Fig. 10 (b) shows the SER performance of the proposed OSM with the spatial area division strategy, where the spatial subchannel correlation between the two LED groups is reduced through controlling the semi-angle at the half power of the LED, and the receiver is located at the coverage area of the first LED group. In the proposed spatial area division strategy, only one data stream is transmitted in a specific coverage area. Under the same data rate, the SER performance of the spatial area division strategy is better than that of the multiple data stream scheme when the data rate is 400Mbps or 600Mbps. That is because the spatial subchannels of the MIMO VLCs are correlated, and the degree of freedom of the MIMO channel is low. However, when the data rate increases to 800Mbps, the multiple data stream scheme achieves better performance because of the high modulation order (256-PAM) employed in the spatial area division strategy. Therefore, we can adaptively adjust the alignment angle and the semiangle at the half power of the LED, and control the coverage area of different LED groups, according to the data rate requirements.

VII. CONCLUSION

This paper proposed a low-complexity OSM scheme based on bipolar PAM for high-rate indoor VLC systems. Under the nonnegative constraint of IM/DD VLCs, the polarity of the signal is mapped to the index of LEDs, and a new PAM constellation diagram  designed by

making use of the spatial elements. Based on the transmit strategy, a novel receive algorithm was proposed. Simulation results showed that the proposed scheme performs the best with SNR gains over reference schemes ranging from 1.5 to 7 dB at a BER of 10^{-4} , when the correlation between the spatial subchannels is low. Especially, compared with the DCO-OFDM based OSM employing the optimal detector, the proposed scheme performs better in the high SNR region, and has a lower computational complexity and PAPR. When the spatial subchannels are highly correlated, a spatial division strategy was applied to reduce the effect of the high correlation of spatial subchannels, and it achieves good BER performance.

APPENDIX A

STATISTIC PROPERTIES OF $A(K)$ AND $D(K)$

It is assumed that $\alpha_j(n)$ is a random variable with zero mean and variance σ_α^2 , and the expected value of $|\alpha_j(n)|$ is $E[|\alpha_j(n)|] = p_{|\alpha|}$. Therefore,

$$E[(|\alpha_j(n)|)^2] = E[(\alpha_j(n))^2] = \sigma_\alpha^2. \quad (\text{A.1})$$

According to the definition of IDFT, $A_j(K)$ and $D_j(K)$ can be expressed as

$$\begin{cases} A_j(K) = \sum_{n=0}^{N-1} \alpha_j(n) e^{-j\frac{2\pi}{N}Kn} \\ D_j(K) = \sum_{n=0}^{N-1} |\alpha_j(n)| e^{-j\frac{2\pi}{N}Kn} \end{cases}. \quad (\text{A.2})$$

According to the law of large numbers [40], $A_j(K)$ is a zero mean Gaussian random variable with variance $N\sigma_\alpha^2$. The mean of $D_j(K)$ is

$$E[D_j(K)] = \begin{cases} Np_{|\alpha|}, & K = 0 \\ 0, & K = 1, 2, \dots, N-1 \end{cases}. \quad (\text{A.3})$$

The variance of $D_j(K)$ ($K = 0, 1, \dots, N-1$) is

$$\begin{aligned} \text{var}\{D_j(K)\} &= N \text{var}\{|\alpha_j(n)|\} \\ &= N(\sigma_\alpha^2 - p_{|\alpha|}^2). \end{aligned} \quad (\text{A.4})$$

REFERENCES

- [1] T. Komine and M. Nakagawa, "Fundamental analysis for visible-light communication system using LED lights," *IEEE Trans. Consumer Electronics*, vol. 50, no. 1, pp. 100–107, Feb. 2004.
- [2] Q. Gao, R. Wang, Z. Xu, and Y. Hua, "DC-informative joint color-frequency modulation for visible light communications," *J. Lightwave Tech.*, vol. 33, no. 11, pp. 2181–2188, Jun. 2015.
- [3] H. Elgala, R. Mesleh, and H. Haas, "Indoor optical wireless communication: Potential and state-of-art," *IEEE Commun. Mag.*, vol. 49, no. 9, pp. 56–62, Sept. 2011.
- [4] F. Jin, R. Zhang, and L. Hanzo, "Resource allocation under delay-guarantee constraints for heterogeneous visible-light and RF femtocell," *IEEE Trans. Wirel. Commun.*, vol. 14, no. 2, pp. 1020–1034, Feb. 2015.
- [5] L. Wu, Z. Zhang, J. Dang, and H. Liu, "Adaptive modulation schemes for visible light communications," *J. Lightwave Tech.*, vol. 33, no. 1, pp. 117–125, Jan. 2015.
- [6] J. M. Kahn and J. R. Barry, "Wireless infrared communications," *Proc. IEEE*, vol. 85, no. 2, pp. 265–298, Feb. 1997.
- [7] T. Ohtsuki, "Multiple-subcarrier modulation in optical wireless communication," *IEEE Commun. Mag.*, vol. 41, no. 3, pp. 74–79, Mar. 2003.
- [8] J. Armstrong and A. Lowery, "Power efficient optical OFDM," *Electron. Lett.*, vol. 42, no. 6, pp. 370–372, Mar. 2006.
- [9] J. Armstrong, B. Schmidt, D. Kalra, H. A. Suraweera and A. J. Lowery, "Performance of asymmetrically clipped optical OFDM in AWGN for an intensity modulated direct detection system," in *Proc. IEEE GLOBECOM 2006*, San Francisco, CA, Nov./Dec. 2006, pp. 1-5.
- [10] S. Dissanayake and J. Armstrong, "Comparison of ACO-OFDM, DCO-OFDM and ADO-OFDM in IM/DD systems," *J. Lightwave Tech.*, vol. 31, no. 7, pp. 1063–1072, April 2013.
- [11] S. C. J. Lee, S. Randel, F. Breyer and A. M. J. Koonen, "PAM-DMT for intensity-modulated and directd detection optical communication systems," *IEEE Photonics Technol. Lett.*, vol. 21, no. 23, pp. 1749–1751, Dec. 2009.
- [12] D. J. F. Barros, S. K. Wilson and J. M. Kahn, "Comparison of orthogonal frequency-Division multiplexing and pulse-Amplitude modulation in indoor optical wireless links," *IEEE Trans. on Commun.*, vol. 60, no. 1, pp. 153–163, Jan. 2012.
- [13] N. Fernando, H. Yi, and E. Viterbo, "Flip-OFDM for unipolar communication systems," *IEEE Trans. Commun.*, vol. 60, no. 12, pp. 3726–3733, Dec. 2012.
- [14] D. Takase and T. Ohtsuki, "Optical wireless MIMO communications (OMIMO)," in *Proc. IEEE GLOBECOM'04*, vol. 2, Dec. 2004, Texas, USA, pp. 928–932.
- [15] L. Zeng, D. O'Brien, H. Minh, G. Faulkner, K. Lee, D. Jung, Y. Oh, and E. T. Won, "High data rate multiple input multiple output (MIMO) optical wireless communications using white LED lighting," *IEEE J. Select. Areas Commun.*, vol. 27, no. 9, pp. 1654–1662, Dec. 2009.
- [16] J. Armstrong, "Alamouti coding for indoor optical wireless communications using ACO-OFDM," in *Proc. 43rd Asilomar Conf. Signals, Systems and Computers*, 2009, pp. 1650–1654.
- [17] G. Ntogari, T. Kamalakis, and T. Sphicopoulos, "Performance analysis of space time block coding techniques for indoor optical wireless system," *IEEE J. Select. Areas Commun.*, vol. 27, no. 9, pp. 1545–1552, Dec. 2009.
- [18] R. Mesleh, H. Haas, S. Sinanovic, C. W. Ahn, and S. Yun, "Spatial modulation," *IEEE Trans. Veh. Technol.*, vol. 57, no. 4, pp. 2228–2241, July 2008.
- [19] T. Fath and H. Haas, "Performance comparison of MIMO techniques for optical wireless communications in indoor environments," *IEEE Trans. Commun.*, vol. 61, no. 2, pp. 733–742, Feb. 2013.

- [20] R. Mesleh, H. Elgala, and H. Haas, "Optical spatial modulation," *J. Opt. Commun. Netw.*, vol. 3, no. 3, pp. 234–244, Mar. 2011.
- [21] A. Yesilkaya, E. Basar, F. Miramirkhani, E. Panayirci, M. Uysal, and H. Haas, "Optical MIMO-OFDM With Generalized LED Index Modulation," *IEEE Transactions on Communications*, vol. 65, no. 8, pp. 3429–3441, Aug. 2017.
- [22] R. Tejaswi, T. Lakshmi Narasimhan, and A. Chockalingam, "Quad-LED complex modulation (QCM) for visible light wireless communication," *Proc. IEEE WCNC 2016*, Doha, Qatar, Apr. 3-6, 2016, pp. 1–6.
- [23] T. Lakshmi Narasimhan, R. Tejaswi, and A. Chockalingam, "Quad-LED and dual-LED complex modulation for visible light communication," <https://arxiv.org/pdf/1510.08805.pdf>.
- [24] L. Wu, J. Cheng, Z. Zhang, J. Dang, and H. Liu, "Low-complexity spatial modulation for IM/DD optical wireless communications," *IEEE Photon. Technol. Lett.*, vol. 31, no. 6, pp. 475–478, Mar. 2019.
- [25] J. Wang, S. Jia, and J. Song, "Generalised spatial modulation system with multiple active transmit antennas and low complexity detection scheme," *IEEE Trans. Wireless Commun.*, vol. 11, no. 4, pp. 1605–1615, Apr. 2012.
- [26] P. Yang, M. Di Renzo, Y. Xiao, S. Li, and L. Hanzo, "Design guidelines for spatial modulation," *IEEE Commun. Surveys Tuts.*, vol. 17, no. 1, pp. 6–26, 1st Quart. 2015.
- [27] L. Wu, Z. Zhang and H. Liu, "MIMO-OFDM visible light communications system with low complexity," in *Proc. IEEE ICC'13*, June 2013, Budapest, Hungary, pp. 2526–2530.
- [28] Y. Li, D. Tsonev, and H. Haas, "Non-DC-biased OFDM with optical spatial modulation," in *Proc. IEEE PIMRC'13*, Sep. 2013, London, UK, pp. 486–490.
- [29] H. Olanrewaju, J. Thompson, and W. Popoola, "Performance of optical spatial modulation in indoor multipath channel," *IEEE Trans. Wireless Commun.*, vol. 17, no. 9, pp. 6042–6052, Sept. 2018.
- [30] V. Jungnickel, V. Pohl, S. Nonnig, and C. V. Helmolt, "A physical model of the wireless infrared communication channel," *IEEE J. Sel. Areas Commun.*, vol. 20, pp. 631–640, Aug. 2002.
- [31] S. Long, A. Khalighi, M. Wolf, S. Bourennane, Z. Ghassemlooy, "Investigating Channel Frequency Selectivity in Indoor Visible Light Communication Systems," *IET Optoelectronics*, vol. 10, no. 3, pp. 80–88, May 2016.
- [32] L. Zeng, D. O'Brien, H. Le-Minh, et al, "Improvement of data rate by using equalization in an indoor visible light communication system," in *Proc. IEEE ICCSC 2008*, May 2008, pp. 678–682.
- [33] H. J. Blinichikoff, and A. I. Zverev, *Filtering in the time and frequency domains*, SciTech Publishing Inc., 2001.
- [34] D. C. O'Brien and M. Katz, "Optical wireless communications within fourth-generation wireless systems," *J. Optical Networking*, vol. 4, no. 6, pp. 312–322, June 2005.
- [35] S. Dimitrov and H. Haas, "Information rate of OFDM-based optical wireless communication systems with nonlinear distortion," *J. Lightwave Tech.*, vol. 31, no. 6, pp. 918–929, Mar. 2013.
- [36] J. Proakis, *Digital Communications*. 4th ed. New York: McGraw-Hill, 2001.
- [37] Y. Jiang, M. K. Varanasi, and J. Li, "Performance analysis of ZF and MMSE equalizers for MIMO systems: An in-depth study of the high SNR regime," *IEEE Trans. Inf. Theory*, vol. 57, no. 4, pp. 2008–2026, Apr. 2011.
- [38] D. Tse and P. Viswanath, *Fundamentals of wireless communication*. Cambridge University Press, 2005.
- [39] X. Li, Fan Jin, R. Zhang, J. Wang, Z. Xu, and L. Hanzo, "Users First: User-Centric Cluster Formation for Interference-Mitigation in Visible-Light Networks," *IEEE Trans. Wirel. Commun.*, vol. 15, no. 1, pp. 39–53, Jan. 2016.
- [40] J. Armstrong and B. J. C. Schmidt, "Comparison of asymmetrically clipped optical OFDM and DC-biased optical OFDM in AWGN," *IEEE Commun. Lett.*, vol. 12, no.5, pp. 343–345, May 2008.